All-fiber ring-cavity based frequency swept laser source for frequency domain OCT

Minghui Chen (陈明惠)[1], Zhihua Ding (丁志华)[1*], Lei Xu (徐 磊)[1], Tong Wu (吴 彤)[1], Chuan Wang (王 川)[1], Guohua Shi (史国华)[2], and Yudong Zhang (张雨东)[2]

[1]*State Key Lab of Modern Optical Instrumentation, Zhejiang University, Hangzhou 310027, China*

[2]*Institute of Optics and Electronics, Chinese Academy of Sciences, Chengdu 610209, China*

[*]*E-mail: zh_ding@zju.edu.cn*

Received April 9, 2009

We develop a high-speed tunable, quasi-continuous-wave laser source for frequency domain (FD) optical coherence tomography (OCT). The laser resonance is realized within a unidirectional all-fiber ring cavity consisting of a fiber coupler, two fiber isolators, a semiconductor optical amplifier (SOA), and a fiber Fabry-Perot tunable filter (FFP-TF) for frequency tuning. Light output from the coupler is further amplified and spectral shaped by a booster SOA terminated at both ends with two isolators. The developed laser source provides up to 8000 sweeps per second over a full-width wavelength tuning range of 120 nm at center wavelength of 1320 nm with an average power of 9 mW, yielding an axial resolution of 13.6 μm in air and a maximum sensitivity of about 112 dB for OCT imaging. The instantaneous linewidth is about 0.08 nm, enabling OCT imaging over an axial range of 3.4 mm in air. For optimization consideration based on this custom-built swept laser, experimental study on imaging quality relevant parameters of the swept laser with sine and ramp driving waveforms to the FFP-TF is conducted, and investigation of the swept laser on the cavity length is done. Implementing the laser source in our established swept source based OCT (SS-OCT) system, real-time structural imaging of biological tissue is demonstrated.

OCIS codes: 170.4500, 230.6080, 140.3460.

doi: 10.3788/COL20100802.0202.

Optical coherence tomography (OCT) which is a non-invasive, non-contact imaging modality enables cross sectional imaging of tissues with micron scale resolution[1]. Frequency domain OCT (FD-OCT), different from time domain OCT (TD-OCT), obtains full depth profile by Fourier transform of the interference spectra with a static reference arm[2−4]. FD-OCT can be classified by spectral domain OCT (SD-OCT) and swept source OCT (SS-OCT). In a SD-OCT system, a broadband light source is used and the interference spectral components are measured in a spectrometer by a high-speed charge-coupled device (CCD). Alternatively, in a SS-OCT system, a high-speed tunable, continuous-wave (CW) laser source is used and the interference spectral signal is detected by a single detector. Compared with SD-OCT, SS-OCT has the advantages of point detection and narrow instantaneous linewidth without crosstalk, resulting in a large imaging depth range. Reliable swept laser source is the key component and crucial technology in the development of SS-OCT, especially around 1300- and 1000-nm wavelength ranges where low cost CCDs are not available[5−8]. Therefore, the development of high-speed swept laser source causes great attention and becomes one of the hot areas in biomedical imaging in recent years.

Since Chinn *et al.* obtained the first SS-OCT images of glass cover slips using a grating-tuned external cavity super luminescent light emitting diode (LED) with a peak gain at 840 nm[9], different swept laser sources for SS-OCT have been demonstrated. Elements such as acousto-optic tunable filter (AOTF), rotating galvanometer mirror or polygon mirror with diffraction grating filter, and fiber Fabry-Perot tunable filter (FFP-TF) have been used for frequency tuning[10−13]. Huber *et al.* developed a Fourier domain mode-locked (FDML) swept laser based on a FFP-TF providing a sweeping rate up to several hundred kilohertzs[14−16]. The FDML swept source is superior in achieving scanning speed up to several hundred kilohertzs. However, such mechanism requires very long fiber ring-cavity length up to several tens of kilometers, and fiber dispersion and temperature-dependent ring-cavity length variations must be carefully managed. Therefore, the short ring-cavity length swept source structure first proposed by Huber *et al.* is adopted in this letter[13]. Such short ring-cavity length swept source with moderate scanning speed is robust, easy to maintain and miniaturize, making it suitable for point-of-care applications. We develope a homemade all-fiber short ring-cavity length swept laser without any free space beam paths based on a fiber coupled semiconductor optical amplifier (SOA), a FFP-TF, and an additional fiber coupled booster SOA for spectrum modification and power enhancement. Implementing this swept laser source in our established SS-OCT system, real-time structural imaging of biological tissue is demonstrated. Custom-built swept laser source instead of a commercial one interfacing with OCT system offers more degrees of freedom in the optimization of imaging quality and system. For optimization consideration, experimental study on imaging quality relevant parameters of the swept laser with sine and ramp driving waveforms to the FFP-TF is conducted, and investigation of the swept laser on the cavity length is done.

Figure 1 illustrates the schematic diagram of the all-fiber ring-cavity based frequency swept laser. The ring-cavity consists of two isolators, a fiber coupled SOA, a

piezoelectric actuated FFP-TF, and a coupler. The fiber coupled SOA (InPhenix Inc.) with a gain maximum centered around 1300 nm is polarization independent. The gain SOA provides fiber-to-fiber small-signal gain of 22.2 dB with saturation output power of 9.0 dBm. Two isolators are used to eliminate all extraneous intra-cavity reflections and ensure unidirectional lasing of the ring cavity. The FFP-TF (Micro Optics Inc.) acts as a narrow-band transmission filter for active wavelength selection. The FFP-TF has a free spectral range (FSR) of 184.1 nm, a bandwidth of 0.103 nm, and an insertion loss of 0.6 dB, covering the complete spectral tuning range of the laser source. The high finesse of the FFP-TF makes narrow-band spectral filtering suitable for achieving a sufficient coherence length. The function generator used as the waveform driver is applied to the piezoelectric transducer (PZT, impedance capacity of about 2.2 μF) within the FFT-TF. Fourty percent of the power in the ring-cavity is coupled out by the fiber coupler. After isolation, the output from the fiber coupler is further amplified by a second fiber coupled SOA (InPhenix Inc.) acting as a booster amplifier. The amplified stimulated emission (ASE) optical spectra of the gain SOA and the booster SOA are illustrated in Fig. 2. It is shown that the booster SOA with red shift spectrum and higher power than the gain SOA while almost the same bandwidth. The final isolator terminated at the output is used to avoid reflection from application system back to the ring-cavity.

The output spectra of the developed laser source with and without booster SOA driven by ramp wave to the intra-cavity FFP-TF are shown in Fig. 3. The gain SOA and the booster SOA are both driven at 300-mA current bias, and a ramp driving waveform at frequency of 4 kHz is applied to the FFT-TF for frequency tuning. For comparability of the measured spectral intensity, the

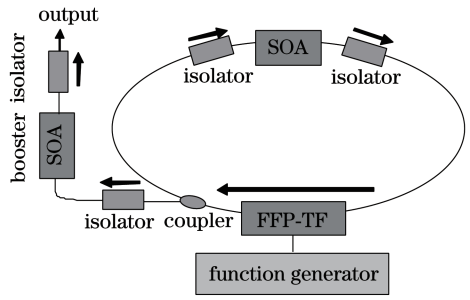

Fig. 1. Schematic diagram of the all-fiber ring-cavity based swept laser source.

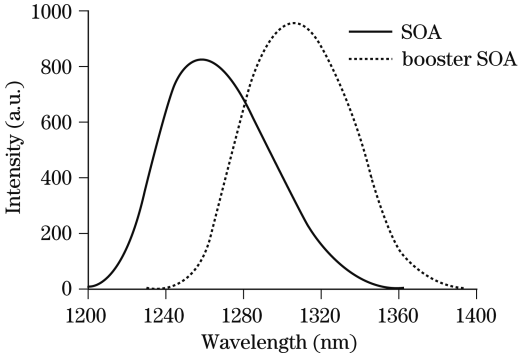

Fig. 2. ASE spectra of the gain SOA and the booster SOA.

spectra are measured with a spectrometer at different gain settings. The laser without the booster SOA provides a tuning range of 73 nm and a full-width at half-maximum (FWHM) bandwidth of 58 nm at the center wavelength of 1310 nm. Comparatively, the laser with the booster SOA provides a tuning range of 120 nm and a FWHM bandwidth of 65 nm at the center wavelength of 1320 nm. It is evident that the original asymmetric spectrum is not only well shaped but also considerably broadened with red-shifted center wavelength by the booster SOA. Furthermore, the average power is amplified largely from 0.8 to 9 mW. To compare the imaging quality relevant parameters of the swept laser with different driving waveforms to the intra-cavity FFP-TF, sine wave is also used to drive the intra-cavity FFP-TF. The output spectrum corresponding to sine wave is also shown in Fig. 3. It can be seen that the spectrum corresponding to ramp wave is broader than that by sine wave. What is more, the output power when driven by sine wave is a little bit lower than that when driven by ramp wave.

Figure 4 shows that the normalized transient intensity profiles of the developed laser source with and without booster SOA. For response consideration, the temporal

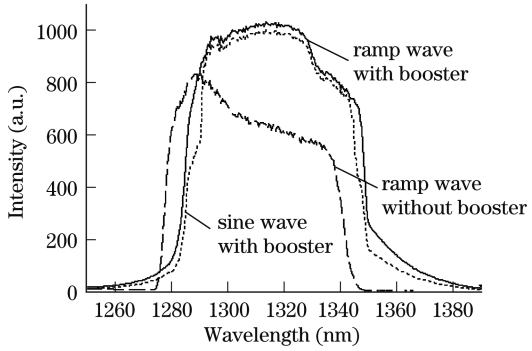

Fig. 3. Output spectra of the swept laser for different driving waveforms with and without booster SOA.

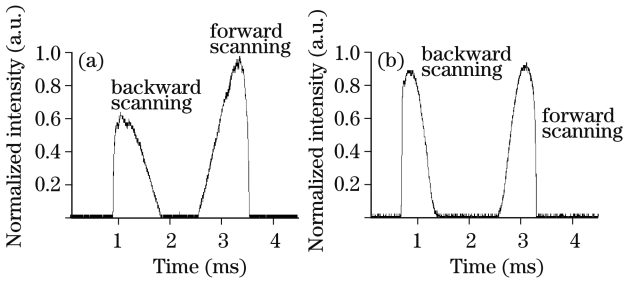

Fig. 4. Normalized temporal intensity profiles of the swept laser (a) without and (b) with booster SOA at the driving frequency of 200 Hz.

Table 1. Measured Parameters of Swept Laser before and after the Shortening of the Ring-Cavity

Length (m)	f_s (kHz)	$P_{w/o}$ (mW)	P_w (mW)
10	8	0.8	9.0
10	12	0.3	7.7
8	12	0.8	9.2

intensity profiles are recorded at a low driving frequency of 200 Hz. In case of ramp driving waveform applied to the FFT-TF, frequency swept rate is twice the driving frequency accounting for both forward and backward tuning. Therefore, 8-kHz frequency swept rate is realized for OCT imaging if both forward (scanning from shorter to longer wavelengths) and backward (scanning from longer to shorter wavelengths) frequency tuning schemes are used. It is observed that forward tuning is favored compared with backward tuning, as shown in Fig. 4(a), where spectral intensity is lower during backward tuning than that during forward tuning. The reason might be related to the four-wave mixing in SOA which has a tendency of downshifting. Comparing Fig. 4(b) with (a), it is noticed that the booster SOA not only enhances the output power, but also modifies the output spectral shape as well as its spectral bandwidth which are important for the improvement of the axial resolution of the reconstructed images in SS-OCT.

The maximum achievable tuning speed of frequency is inversely proportional to the cavity length. In order to investigate the performance of the swept laser on its cavity length, we simply reduce the ring-cavity length to 8 m by removing the second isolator within the intracavity shown in Fig. 1. Table 1 illustrates the measured parameters of swept laser before and after the shortening of the ring-cavity, where f_s is the tuning frequency of the swept source, $P_{w/o}$ and P_w are the output powers of the laser source without and with booster SOA, respectively. The output power decreases significantly as the tuning frequency is increased from 8 to 12 kHz for a constant cavity length of 10 m. However, by reducing the ring-cavity length to 8 m, there is no degradation of the output power when the tuning frequency is increased from 8 to 12 kHz.

The schematic of the SS-OCT system based on the developed swept laser is illustrated in Fig. 5. The only difference from previous system is the homemade swept laser source used instead of the high cost commercial source (HSL-2000, Santec Inc.)[17,18]. SS-OCT system is basically a Michelson interferometer with balanced detection scheme. The reference arm is composed of a polarization controller (PC), a fiber collimator, focusing lenses, and a plane reflecting mirror (RM). OCT imaging is performed by using a beam scanning system consisting of a fiber collimator, an achromatic lens of 40-mm focal length, and an electrical motorized translation stage. Then, balance photodiode detector (BPD) detects interference light signal and converts it into voltage signal. One analog input channel of data acquisition (DAQ, NI5122, National Instruments Inc.) digitizes the voltage signal. For real-time frequency recalibration, a fraction of the laser output power is split off into a Mach-Zender interferometer (MZI), and then the nearest neighbor check algorithm is implemented to obtain N sample points which are equal frequency spaced. The recalibration signal is recorded on the second channel of the DAQ synchronously with the sample signal from the OCT interferometer, allowing real-time recalibration of the interference signal for equal spacing in frequency through the FFT algorithm. After data processing and reconstruction, tomographic images of samples are acquired.

To evaluate the performance of the SS-OCT system based on the developed swept laser driven by ramp and sine waves, a plane RM is firstly used as the sample to measure the point spread function (PSF) of the system. Figures 6(a)–(c) show the interference spectra of the plane RM and corresponding axial PSFs with the FFP-TF driven by sine and ramp waveforms, respectively.

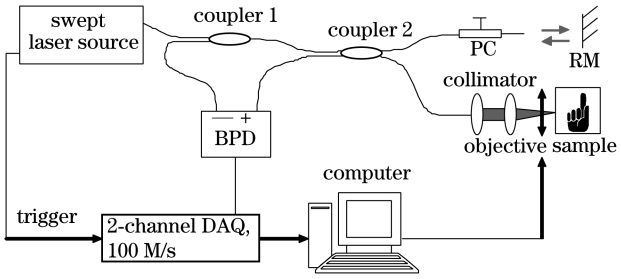

Fig. 5. Schematic of the SS-OCT system based on the developed swept laser source.

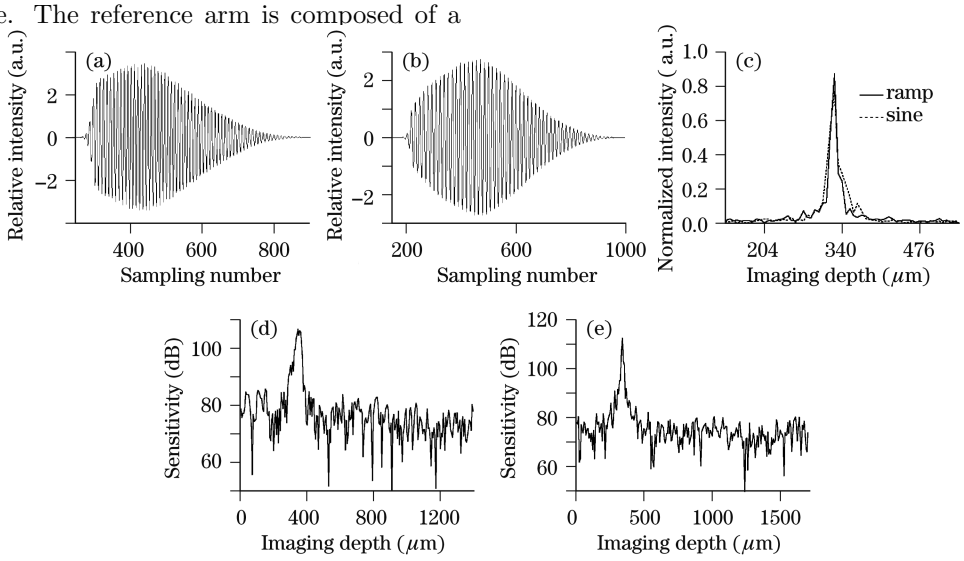

Fig. 6. Interference spectra of plane RM with the FFP-TF driven by (a) sine and (b) ramp waveforms; (c) PSF of the SS-OCT system at imaging depth of 326 μm with the FFP-TF driven by sine (dot) and ramp (line) waveforms; sensitivity of the SS-OCT system with the FFP-TF driven by (d) sine and (e) ramp waveforms.

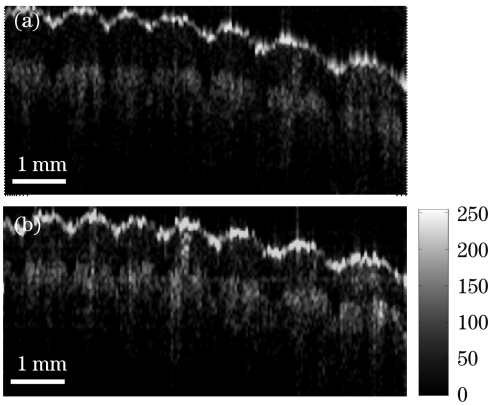

Fig. 7. *In vivo* OCT images of human finger obtained by the SS-OCT based on the developed swept source with the FFP-TF driven by (a) sine and (b) ramp waveforms.

The axial resolution from measured PSF when driven by ramp waveform is 13.6 μm in air (9.7 μm in tissue), approximating the expected value of 11.8 μm. The main reason for this discrepancy is caused by calibration error in wavelength based on MZI method. Such difference between measured resolution and the expected one is also found in our previous work where the same MZI calibration method was implemented[18]. It is clear that the resolution for ramp driving waveform is higher than that for sine driving waveform (17.0 μm). There are two aspects accounting for this difference. Firstly, the shapes of spectra characterized by center wavelength and FWHM bandwidth are different for sine and ramp driving signals. As shown in Fig. 3, the FWHM bandwidth of spectrum corresponding to ramp wave is broader than that by sine wave. Secondly, ramp driving function is superior to sine driving function in linearity of temporal wavelength scanning, which benefits correct recording of interference spectrum under the same sampling frequency of DAQ, and hence less resolution degradation.

The sensitivity of the SS-OCT system with different driving waveforms applied to the FFP-TF is demonstrated in Figs. 6(d) and (e). The maximum sensitivities at a depth of 326 μm are 108 and 112 dB corresponding to sine and ramp waves, respectively. Superior sensitivity is achieved when ramp waveform instead of sine waveform is applied to the intra-cavity FFP-TF.

The resolution and sensitivity advantages of swept source driven by ramp waveform over sine waveform are further confirmed by OCT images of human finger. As shown in Fig. 7, higher resolution and better image quality are achieved in the case of ramp waveform than that driven by sine waveform.

In conclusion, a frequency swept laser source at sweeping speed up to 8 kHz is developed. The sweep speed of 12 kHz is obtained by shortening the ring-cavity to 8 m. The laser centered at 1320 nm is capable of tuning at full-width range of 120 nm, 3-dB range of 65 nm, and the linewidth is about 0.08 nm. The average output power of 9 mW is achieved if a booster SOA is implemented. The booster SOA not only significantly increases the output power of the source, but also shapes its spectrum for better OCT imaging. The laser source is fully fiber-based, having no free optical paths, and hence robust and stable. Implementing this homebuilt swept laser source instead of the commercial one in our existing SS-OCT system, real-time structural imaging of human finger from volunteer with an axial resolution of 9.7 μm is achieved and the maximum sensitivity is about 112 dB. Higher resolution and sensitivity imaging is confirmed in the case of ramp driving waveform in comparison with sine driving waveform, which demonstrates that an optimization of imaging quality could be realized by applying appropriate driving waveform to the FFP-TF. However, if the required driving frequency is beyond the response capability of the driver, sine wave is a better choice for driving the FFP-TF due to the time response merit of sine wave over ramp wave at the same sampling frequency. It is believed that this short ring-cavity swept source is promising for miniaturization, making it suitable for point-of-care applications.

This work was supported by the National High Technology Research and Development Program of China (Nos. 2006AA02Z4E0 and 2008AA02Z422) and the National Natural Science Foundation of China (Nos. 60878057 and 60478040).

References

1. D. Huang, E. A. Swanson, C. P. Lin, J. S. Schuman, W. G. Stinson, W. Chang, M. R. Hee, T. Flotte, K. Gregory, C. A. Puliafito, and J. G. Fujimoto, Science **254,** 1178 (1991).
2. R. Leitgeb, C. K. Hitzenberger, and A. F. Fercher, Opt. Express **11,** 889 (2003).
3. X. Liu, X. Li, D.-H. Kim, I. Ilev, and J. U. Kang, Chin. Opt. Lett. **6,** 889 (2008).
4. Q. Gong, C. Fan, F. Zhang, and J. Yao, Chin. Opt. Lett. **6,** 905 (2008).
5. K. Wang and Z. Ding, Chin. Opt. Lett. **6,** 902 (2008).
6. B. Liu and M. E. Brezinski, J. Biomed. Opt. **12,** 044007 (2007).
7. L. Ai, F. Yuan, and Z. Ding, Chin. Opt. Lett. **6,** 505 (2008).
8. M. A. Choma, M. V. Sarunic, C. Yang, and J. A. Izatt, Opt. Express **11,** 2183 (2003).
9. S. R. Chinn, E. A. Swanson, and J. G. Fujimoto, Opt. Lett. **22,** 340 (1997).
10. S. K. Dubey, G. Sheoran, T. Anna, A. Anand, D. S. Mehta, and C. Shakher, Proc. SPIE **7155,** 71551F (2008).
11. S. H. Yun, C. Boudoux, G. J. Tearney, and B. E. Bouma, Opt. Lett. **28,** 1981 (2003).
12. J. Zhang, Q. Wang, B. Rao, Z. Chen, and K. Hsu, Appl. Phys. Lett. **89,** 073901 (2006).
13. R. Huber, M. Wojtkowski, K. Taira, J. G. Fujimoto, and K. Hsu, Opt. Express **13,** 3513 (2005).
14. R. Huber, M. Wojtkowski, and J. G. Fujimoto, Opt. Express **14,** 3225 (2006).
15. C. M. Eigenwilling, B. R. Biedermann, G. Palte, and R. Huber, Opt. Express **16,** 8916 (2008).
16. M. Y. Jeon, J. Zhang, Q. Wang, and Z. Chen, Opt. Express **16,** 2547 (2008).
17. T. Wu and Z. Ding, Chinese J. Lasers (in Chinese) **36,** 503 (2009).
18. T. Wu, Z. Ding, M. Chen, L. Xu, G. Shi, and Y. Zhang, J. Innovative Opt. Health Sci. **2,** 117 (2009).